buildings

MDPI

Article

Strengthening Effect of the Fixing Method of Polypropylene Band on Unreinforced Brick Masonry in Flexural, Shear, and Torsion Behaviors

Ta Quy Hung [1], Mitsuo Mizoguchi [2,*] and Yuya Takase [2,*]

[1] Division of Engineering, Muroran Institute of Technology, Muroran 050-8585, Japan; 19096011@muroran-it.ac.jp
[2] College of Design and Manufacturing Technology, Muroran Institute of Technology, Muroran 050-8585, Japan
* Correspondence: mitsuo@muroran-it.ac.jp (M.M.); y.takase@muroran-it.ac.jp (Y.T.)

Abstract: Every year, Vietnam faces typhoons accompanied by strong winds. Semi-permanent houses are severely damaged by these winds. We researched a strengthening method using a Polypropylen (PP) band to prevent housing damage caused by strong winds. In this study, we have developed a new method of fixing PP band to bricks. The PP band is sandwiched between two flat steel washers and fastened with steel screws to a plastic plug embedded in the side of the brick. A total of 49 specimens were used to study the influence of the PP band on the flexural, shear, and torsional behaviors of brick masonry. In the flexural tests, the results show that the average load-carrying capacity at ultimate failure and deflection at first crack of the PP band specimens was 1.7 and 1.62 times, respectively, higher than those of non-PP band specimens. In the shear tests, the tests on the strengthened specimens showed an increase in the shear strength for all pre-compression ranges of 0.2–0.6 N/mm^2. However, it was not significant. Similarly, the initial stiffness was not significantly affected by the pre-compression level in both the reinforced and unreinforced cases. In the torsion tests, the improvements in the average load-carrying capacity and deformation ability at the first crack were 1.21 times and 1.47 times, respectively. In the reinforced specimens, at ultimate failure, a slight increase in load was observed, but it did not exceed the initial peak load.

Keywords: Vietnam typhoon; unreinforced brick masonry wall (URM); semi-permanent house; out-of-plane loading; polypropylene (PP) band

Citation: Hung, T.Q.; Mizoguchi, M.; Takase, Y. Strengthening Effect of the Fixing Method of Polypropylene Band on Unreinforced Brick Masonry in Flexural, Shear, and Torsion Behaviors. *Buildings* **2023**, *13*, 2863. https://doi.org/10.3390/buildings13112863

Academic Editor: Binsheng (Ben) Zhang

Received: 15 October 2023
Revised: 11 November 2023
Accepted: 14 November 2023
Published: 15 November 2023

1. Introduction

Vietnam is a country with most of its territory facing the sea. Earthquakes are not considered a high-priority disaster. However, severe winds from typhoons and tropical storms are responsible for extensive damage. For instance, Typhoon Damrey in 2017 resulted in the devastation of 302,783 houses [1] and Typhoon Molave in 2020 destroyed and damaged 188,759 houses [2]. Typhoons alone account for 80% of all disaster-related damage in the country [3]. In addition, the strength and frequency of typhoons have been gradually increasing in recent years [4,5], which creates more risks to humanity and the economy. In the types of houses damaged by typhoons, studies have pointed out that 70% of them are semi-permanent houses with break structures [6,7]. They are concentrated in rural areas, such as towns and villages. Strengthening interventions have been repeatedly documented as effective methods to preserve unreinforced masonry structures and protect human lives.

Nowadays, many methods have been proposed to strengthen masonry structures, such as reinforced concrete, mortar layer, vertical reinforcement, external post-tensioned technique, and external FRP reinforcement methods [8–12]. However, using these methods is difficult for developing countries, such as Vietnam, owing to the high professional knowledge needed and associated costs. Therefore, strengthening methods using Polypropylene

(PP) band materials have emerged as promising alternatives in developing countries. It was initially proposed by Mayorca et al. with the idea of creating a mesh layer and laying it on the wall surface to increase the strength of the wall [13–15]. The results showed that the PP band-strengthened wall did not increase the structural peak strength. But, it improved the performance after crack occurrence and maintained integrity for large deformations. Umair et al. [16] investigated the effect of the PP band and FRP composite on the increases in the strength and deformation capacity of masonry wall panels in diagonal compression and out-of-plane bending tests. The study proved that the FRP + PP band composite is a high-performance composite solution for seismic retrofitting masonry structures and that using the FRP and PP band composites is viable solution for seismic retrofitting URM structures. In studies [17,18], cost-effective materials such as PP bands and steel wire meshes were used to strengthen masonry wallets. The results clearly showed that both strengthening methods effectively delayed the collapse of the structure and enhanced a significant amount of the flexural load-carrying capacity and ductility of the wall.

In the studies mentioned above, there are two ways of strengthening the PP band. In the first method, the PP band was tightened together by clips using tensioners and sealers [18]. This method was effective in strengthening small brick masonry patterns. However, when considering its use on walls, it is difficult to attach the PP band mesh to the wall. Almost all the walls were restrained at three or four edges. Therefore, the PP band mesh cannot wrap the wall at the intersection between the wall and column. In the second method, PP band mesh was created by using a portable ultrasonic welder. Afterwards, holes were drilled through the mortar layers in the wall and small straws/pipes were left embedded at the joints. PP band mesh can be applied to both faces of the wall with the help of connectors, which can be steel wires and PP bands [16]. When using steel wires to fasten the PP band mesh on the wall, as shown in Figure 2a, the hardness at the connection position was low. Additionally, when observed from the form of destruction in Figure 1, it was found that the surface between the mortar bricks or in the mortar layer was often where the cracks first appeared and continued to expand until failure. This raises the problem of damage to the connection position. It effectively reduces the tension ability of the PP band mesh, owing to the simultaneous displacement of both the fixed position and mesh. Therefore, to clarify this issue, we have developed a suitable PP band fixation method to enhance the hardness at the connection position, shown in Figure 2b.

Figure 1. Damaged semi-permanent house in Typhoon Damrey, 2017.

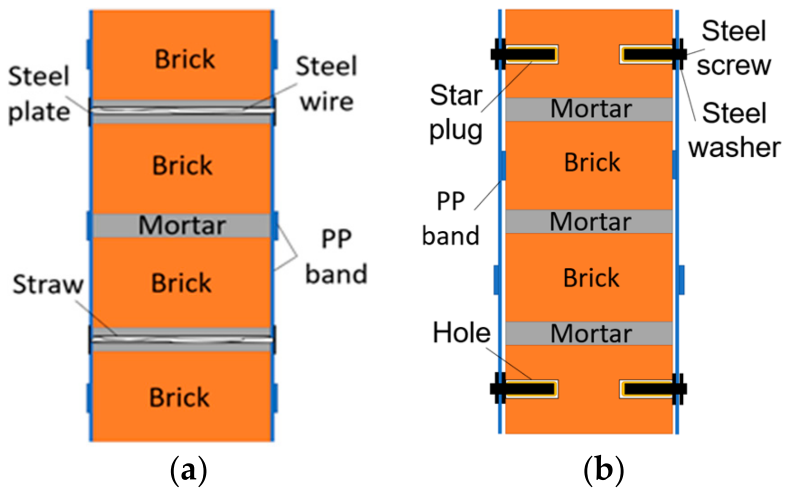

Figure 2. Methods of PP band strengthening. (**a**) Sathiparan et al., 2015 [16]. (**b**) Recent studies.

2. Target Fracture Pattens of Unreinforced Brick Masonry Wall

It is well known that earthquakes are one of the leading causes of the collapse of masonry structures, and the two major seismic-induced damage and collapse models of masonry walls are the in-plane and out-of-plane collapse mechanisms. The URM structures are much weaker in the out-of-plane direction than in the in-plane direction [19]. Out-of-plane loading (perpendicular to the loading direction) is created by wind gusts in typhoons, leading to the collapse of houses. It is more dominant than the in-plane failure of URM walls [20]. However, most masonry walls involved in real semi-permanent houses are supported on three or four sides. These boundary conditions lead to the assumption that the walls are subjected to bi-axial flexion when subjected to out-of-plane loads. The failure models of two-way spanning walls depend on the panel dimensions and support conditions. Consequently, the wall undergoes a combination of horizontal, vertical, and diagonal flexions, which must be investigated (Figure 3).

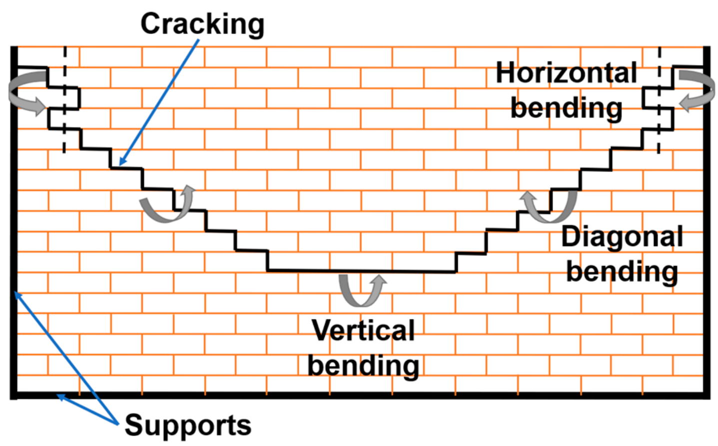

Figure 3. Two-way bending failure modes on the three-edge-supported wall.

Under horizontal bending, vertical cracks can form by two distinct modes and illustrate stepped failure, wherein the crack follows a toothed pattern along the brick–mortar bond of the bed and head joints. The two aspects involved when stepped failure occurs along a stepped crack line are the bending tensile strength of the head joint and the torsional and frictional capacities of the bed joints. Furthermore, in line failure, where the crack cuts across the brick units and head joints in a straight line, the corresponding resistance mechanisms are the bending tensile strength of the head joint and the lateral rupture strength of the brick units. The trend for either mode to be favored depends on the relative material strengths of the brick units and masonry bond. In addition, the failure mode is associated with diagonal bending, which is characterized by the appearance and spread of a diagonal crack in the wall, following the head and bed joints. The strength aspects included in developing a diagonal crack line are the bending tensile strength of the bed joints, torsional and frictional capacities of the bed joints, bending tensile strength of the head joints, and torsional and frictional capacities of the head joints. Regarding vertical bending, a horizontal crack develops along the bed joint, and the strength aspect involved in the appearance of this type is the bending tensile strength or shear strength of the bed joint based on the properties of the brick and masonry bond [21,22]. The mechanisms are quite complex under the bending condition and the distribution of bending moment across the wall, which makes it difficult to assess failure mechanics completely along both the bed joint and head joint. In future, it may be solved by multiscale (e.g., macroscale, microscale, and nanoscale) research, as conducted in Ref [16], but now it is still a problem. Therefore, this study only focused on the failure behaviors of bed joints to investigate the effective strengthening of the PP band on bending, shear, and torsional behaviors using the method developed by the authors. The obtained results will be the necessary parameters to use for numerical modelling of actual walls in subsequent studies.

3. Materials and Methods for Fixing PP Band to Brick

3.1. Materials

3.1.1. Brick and Mortar

Burnt bricks with dimensions of 210 mm × 100 mm × 60 mm (length × width × thickness) were used to construct the specimens according to JIS R1250 [23]. The mechanical properties of the bricks were determined by performing center-point bending, compression, and water absorption tests. The bricks were tested under uniaxial compressive loading (0.0075 mm/s) along the horizontal direction. In further accordance with Vasconcelos and Lourenco [24], Young's modulus of brick (E_b) was also calculated by considering values between 30% and 60% of the compressive strength. Three-point bending tests were also carried out on the brick units at a rate of 0.0075 mm/s in accordance with JIS R2213 [25]. The test results are summarized in Table 1.

Table 1. Mechanical properties of materials.

Type of Material	Properties		Values (COVs)
Brick	Dimension		210 mm × 100 mm × 60 mm
	Density		1.98 g/cm^3
	Water absorption		9% (4.3%)
	Flexural strength		5.2 N/mm^2 (9.8%)
	Compressive strength		36 N/mm^2 (10.3%)
	Young's modulus		15,700 N/mm^2
Ordinary Portland Cement	Density		3.15 g/cm^3
	Specific surface area		3490 cm^2/g
Pit Sand	Density		2.61 g/cm^3
Mortar	Flexural strength Compressive strength Young's modulus	28 days	3.6 N/mm^2 (10.4%) 17.4 N/mm^2 (11.5%) 2400 N/mm^2
		Experiment day	4.7 N/mm^2 (11.7%) 23 N/mm^2 (12.6%)-

Cement mortar was selected with mixed proportions of water/cement (C/S) and cement/sand (C/S) equal to 0.7 and 4.17, respectively. Tap water was used for mixing, and the water temperature was in the range of 25 ± 5 °C. Cement, sand, and water were measured by weight in accordance with their respective proportions. Saturated surface dry sand with a grain size of less than 0.6 mm was used in each mix. The mechanical properties of mortar were evaluated by testing mortar prisms of 40 mm × 40 mm × 160 mm at the age of 28 days and the experiment day. Molding was performed under laboratory conditions. The samples were kept in the steel mold for 24 h after casting, and the samples were removed from the molds after they were kept in the curing water until the date of testing. The flexural strength was measured by means of three-point bending tests according to JIS R5021 [26], whereas the compressive strength was determined on the halves of the specimens after the bending tests. The mechanical properties of the mortar are listed in Table 1 together with the coefficients of variation (COVs) in the parentheses.

3.1.2. Strengthening Material

The specimens were strengthened using a PP band (popularly used as a carton packaging material). We evaluated the tensile properties of PP bands with dimensions 15.5 mm × 0.5 mm × 500 mm (width × thickness × length) according to JIS Z1527:2002 [27]. Figure 4 exhibits the setup used for the tensile test. The properties of the PP bands used in this investigation are listed in Table 2.

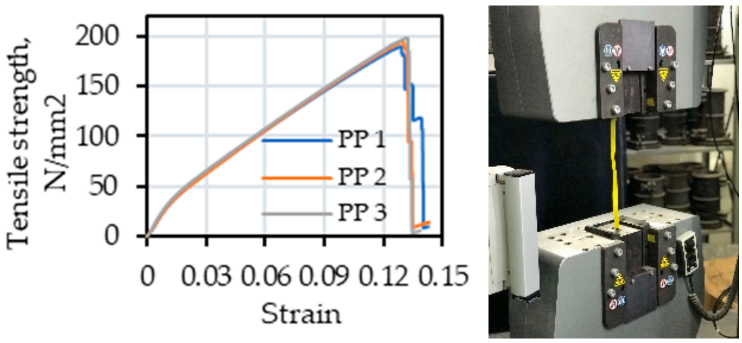

Figure 4. Direct tensile strengths of PP bands.

Table 2. Parameter for PP bands.

Type of Material	Properties	Values
PP band	Width	15.5 mm
	Thickness	0.5 mm
	Density	0.9 g/cm^3
	Tensile strength	194.6 N/mm^2
	Cut-off strain	13.0%
	Modulus of elasticity	1500 N/mm^2

3.2. PP Band Fixing Method to Brick Tests

The installation process is straightforward and does not require skilled labor. The preliminary assessment of the proposed method in the direct tension tests was performed on three cases: (1) using only steel screws (5 mm dia. × 25 mm) (Figure 5a), (2) using steel washers and PP bands placed between the steel washers and bricks joined using steel screws (Figure 5b), (3) using two steel washers with the PP bands placed between them and joined by steel screws (Figure 5c). Each case consists of three specimens with dimensions as shown in Figure 5d. The lengths of the PP bands and loading method were selected in accordance with JIS Z1527:2002 [27]. First, we drilled 6 mm holes in the bricks using an electric drill. The diameters of the holes were sized to ensure a tight fit with the star plugs (6 mm dia. × 25 mm). The tightening force applied to each steel screw was adequate to hold the PP bands firmly in the plane. Figure 5e presents the specimen layouts.

The tensile stress–strain curves for the different investigated cases are presented in Figure 6a–c. It is observed that in Case (1), the average tensile strength and strain were the lowest at 36.5 N/mm^2 and 0.013, respectively (Table 3 and Figure 6a). The PP bands were damaged and separated from the steel screws. Case (2) showed the good bonding ability of the PP bands and rough brick surfaces under the effect of the initial twisting force. The slide in strength of the PP band on the steel washer is also observed in Figure 6b, at a strain range of 0.024 to 0.036. However, in terms of the tensile strength and strain, they were still lower than those in Case (3). In Case (3), the average tensile strength and strain were the highest at 81 N/mm^2 and 0.046 (Table 3 and Figure 6c). It was observed that the connection in Case (3) was the best compared to the other cases. The deformation at the linking part between the steel washers and PP bands does not occur suddenly but is sustained awhile at the edge of the undamaged hole. Therefore, it is advisable to use two steel washers to strengthen the specimens.

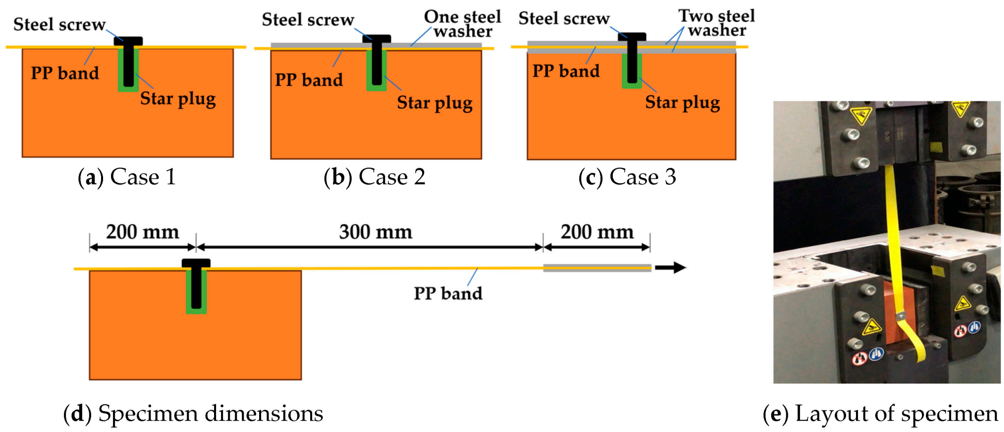

Figure 5. Direct tensile tests at the fixed positions of the PP bands.

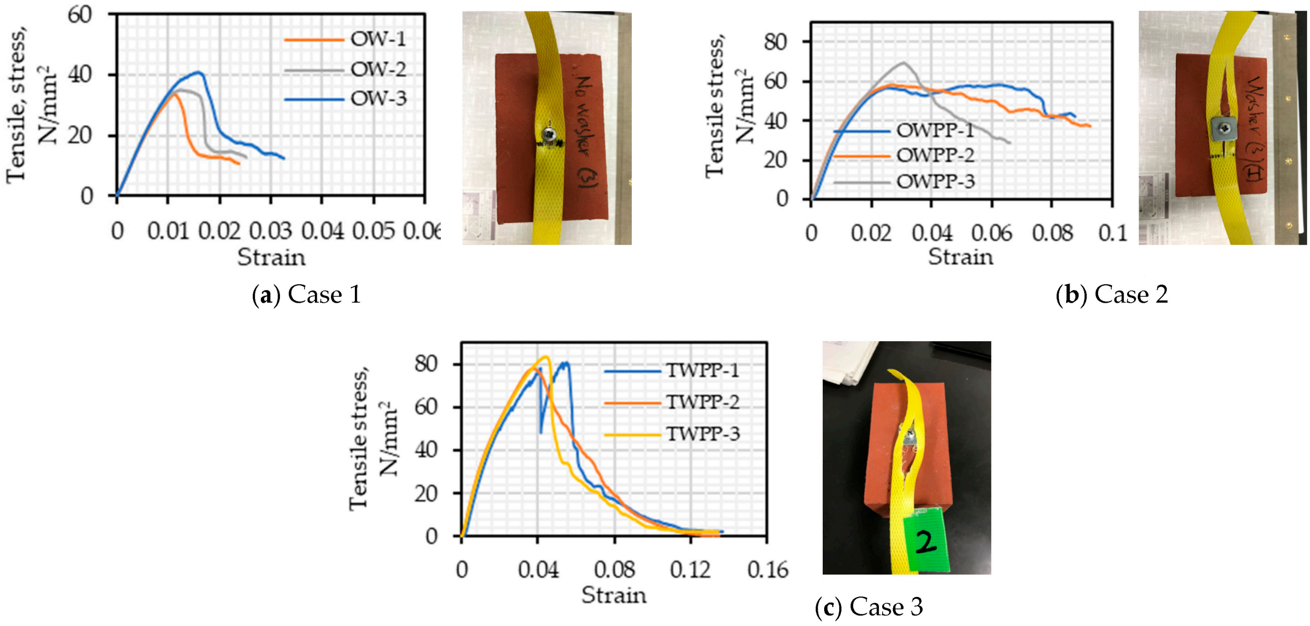

Figure 6. Tensile stress–strain curves and failure patterns in the investigated cases.

Table 3. Tensile test results in the investigated cases.

Case	Sample	Load, N	Tensile Strength, N/mm^2	Strain	Average of Tensile Strength, N/mm^2	Average of Strain
1	OW-1	262	33.7	0.011	36.5	0.013
	OW-2	272	35.1	0.012		
	OW-3	317	40.7	0.016		

Table 3. *Cont.*

Case	Sample	Load, N	Tensile Strength, N/mm^2	Strain	Average of Tensile Strength, N/mm^2	Average of Strain
2	OWPP-1	442	57.0	0.025	61.6	0.028
	OWPP-2	452	58.3	0.027		
	OWPP-3	538	69.4	0.031		
3	TWPP-1	628	81.0	0.055	81.0	0.046
	TWPP-2	607	78.3	0.038		
	TWPP-3	649	83.7	0.045		

4. Experimental Tests

In this study, we conducted flexural, shear, and torsion tests. The details of the tests are explained below.

4.1. Flexural Tests

Nine prism specimens were subjected to flexural failure tests with seven bricklayers and six layers of mortar joints, with dimensions of 480 mm × 210 mm × 100 mm (Figure 7). Four of the nine (FN-1 to FN-4) were not strengthened by the PP bands to determine the flexural tensile strength of the joint and the others (FP-1 to FP-5) were strengthened by the PP bands. Table 4 lists the dimensions of the prism specimens and the distance between supports. The distance between the two fixed PP band positions was approximately equal to the distance between the two PP bands. The tensile force of the PP band when strengthening was created by a hanging scale with a value of 80 N for all specimens. A four-point bending test was performed according to the recommendation of ASTM E518:2010 [28]. The prism specimens were placed horizontally on the support, the distance between supports was maintained at 430 mm (L), and the two-line load was applied by two steel rods with dimensions of 120 mm × 22 mm (length × diameter), with a space of 142 mm, as illustrated in Figure 8. The flexural strength is calculated using Equation (1), as

$$R_{um} = \frac{(P + 0.75P_s) \times L}{b \times d^2} \tag{1}$$

where R_{um} is the ultimate flexural strength, P_s is the self-weight of the prism (N), L is the effective span (mm), b is the average width of the prism (mm), and d is the average depth of the prism (mm).

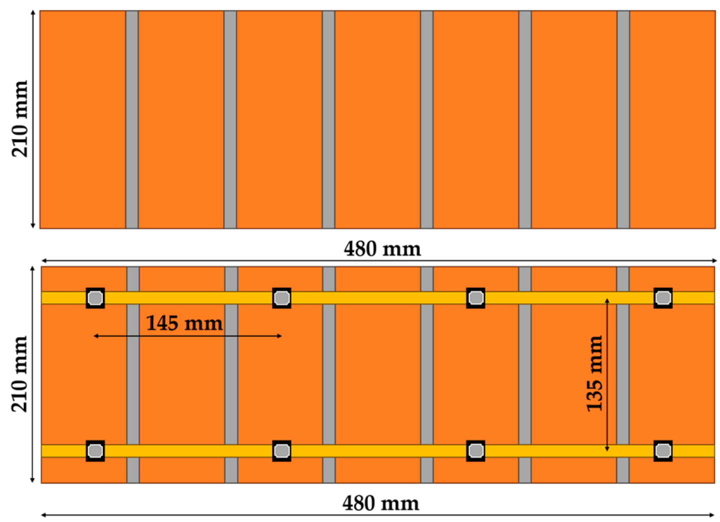

Figure 7. Unreinforced prism specimen and reinforced prism specimen.

Table 4. Dimensions of the prism specimens and the distances between supports.

Numbers		Weight W, N	Span L, mm	Wide b, mm	Depth d, mm
FN-1	Non PP band	200.3	426	210.0	100.0
FN-2		199.8	427	209.5	100.5
FN-3		198.3	427	210.3	100.0
FN-4		198.1	427	209.7	99.80
FP-1	PP band	203.4	432	209.8	100.0
FP-2		200.4	427	211.5	101.2
FP-3		198.1	428	210.0	101.6
FP-4		201.6	430	210.5	100.0
FP-5		205.1	432	210.0	100.0

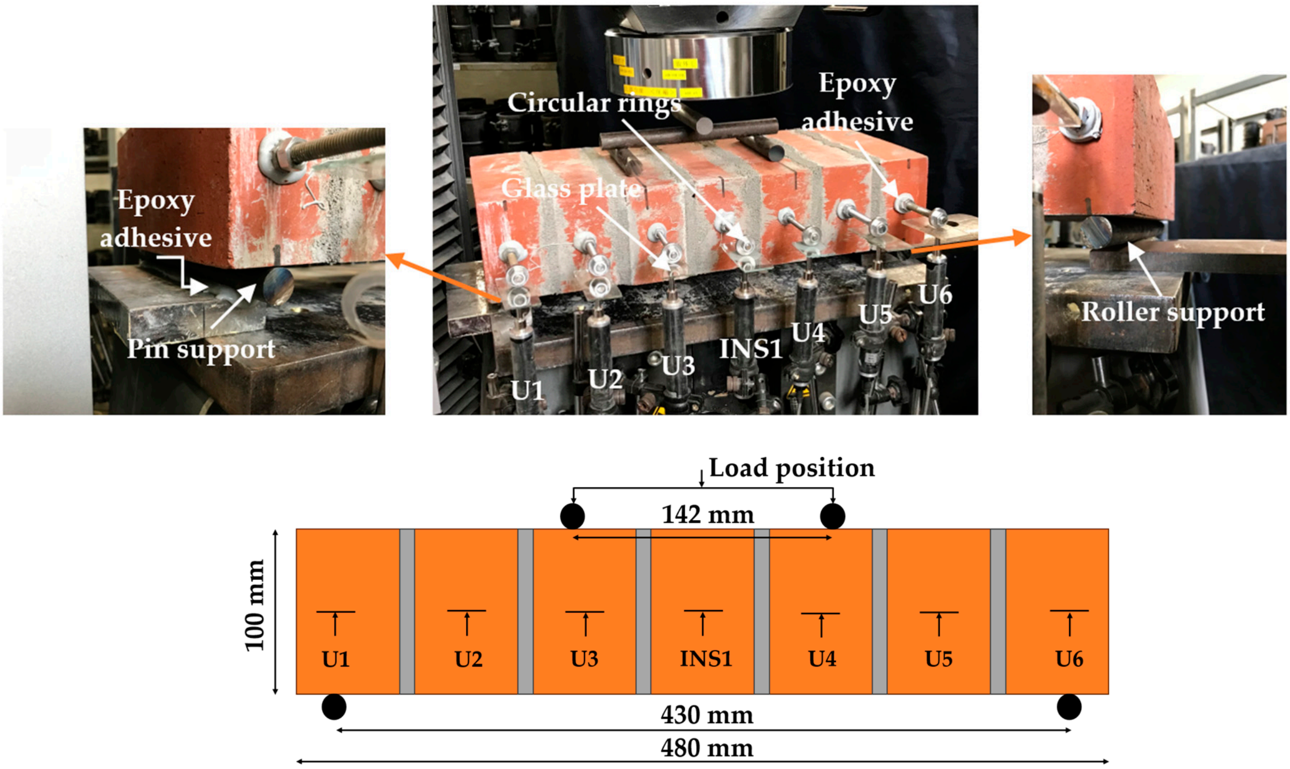

Figure 8. Flexural test set up.

In addition, the mechanical properties, such as stiffness and ductility, were considered because they are critical parameters for determining the efficacy of any strengthening technique in flexural behaviors. The initial stiffness is given by the ratio of the flexural strength to the deflection at the first crack, whereas the secant stiffness is obtained from the ratio of the ultimate flexural strength to the corresponding deflection. Ductility, which is the deformation capacity of a structure before collapse, is evaluated using Equation (2).

$$\mu_\Delta = \frac{\Delta_u}{\Delta_y} \tag{2}$$

where Δ_u and Δ_y are the deflections at ultimate load P_u and cracking load P_y, respectively.

Fourteen linear variable displacement transducers (LVDTs) (U1 to U12; INS1 and INS2) were installed along the horizontal central line of the specimen at two sides to measure the prism displacements during the test, as shown in Figure 8. Two LVDTs (INS1 and INS2) at the specimen center position and load cell were connected to the data acquisition system of the universal testing machine (INSTRON). Due to limitations in the output of the system in Instron, only two LVDTs were used. The others were connected to a fast data logger (U-CAM). The load rate for all prism specimens was kept at 0.005 mm/s. Timing synchronization between the U-CAM and Instron data was performed.

4.2. Shear Tests

Thirty triplet masonry specimens were used in the shear behavior tests. Each triplet specimen was created from three layers of brick and two layers of mortar with the dimensions of 210 mm × 204 mm × 100 mm, as shown in Figure 9. Eighteen out of thirty prisms without PP bands were used to determine the friction angle and cohesion of the mortar joint. Four different levels of pre-compression were used (0 N/mm^2, 0.2 N/mm^2, 0.4 N/mm^2, and 0.6 N/mm^2) in accordance with RILEM TC 127-MS:1996 [29]. The remaining triplet specimens were used to estimate the effects of strengthening with the PP bands in the shear behavior tests. Furthermore, the stiffness of each specimen was ascertained from the stress–slip relationship curve. The strengthening steps for the specimens with PP bands were carried out similarly to those in the flexural test.

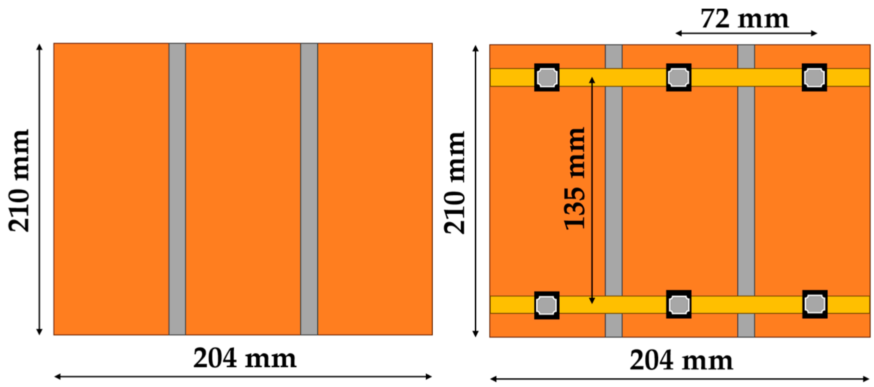

Figure 9. Non-PP band triplet specimen and PP band triplet specimen.

At first, the compressive stress was applied onto the specimen via threaded bars before the shear load was applied. To obtain the pre-compression stress, direct tensile tests of the two threaded bars were initially performed in the elastic region using four strain gauges. The primary purpose was to determine the force–strain relationship in each threaded bar (Figure 10). Prior to conducting the shear behavior test, four strain gauges were connected to the fast data logger (U-CAM) to measure the strains created by the wrench tightening force exerted by the handle (Figure 11a), up to the desired level of axial pre-compression. Two nuts fixed to the bottom steel plate and two threaded bars, and a wooden board and a layer of paperboard were placed at the center of the steel plate. The specimen was placed on a wooden board and compressed by a wrench tightening force using the other two nuts to influence the second steel plate. This ensured diffusion of the compressive load on the entire surface of the specimen. After the pre-compression value was obtained, the specimens were tested in a 500 kN universal testing machine-operated (INSTRON) in displacement control at a rate of 0.0075 mm/s (Figure 11b). The shear load was applied along the vertical direction to the intermediate brick on an area of steel plate of 120 mm × 54 mm. The displacement of each brick was measured using ten LVDTs (U1 to U8; INS1 and INS2) positioned on four sides of the specimens, as shown in Figure 11b.

Triplet specimens were placed such that the applied load acted parallel to the mortar joints. A load was applied as close as possible to the joints. Supports were provided below the triplet specimens at both end units. The shear strength was calculated using Equation (3), as

$$\tau = \frac{P}{A_1 + A_2} \tag{3}$$

where A_1 and A_2 are the areas of the upper and lower mortar joints on the brick surface (mm^2), respectively, and P is the ultimate load.

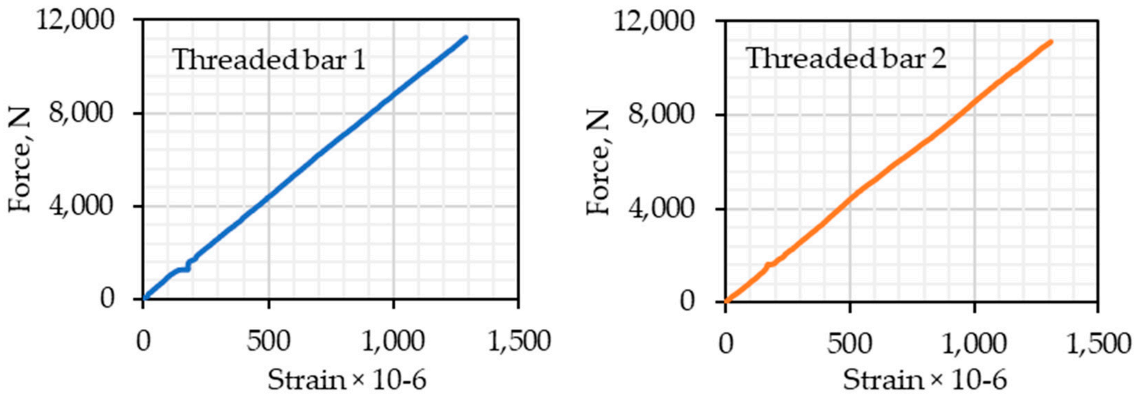

Figure 10. Direct tension force–strain curves of the threaded bars.

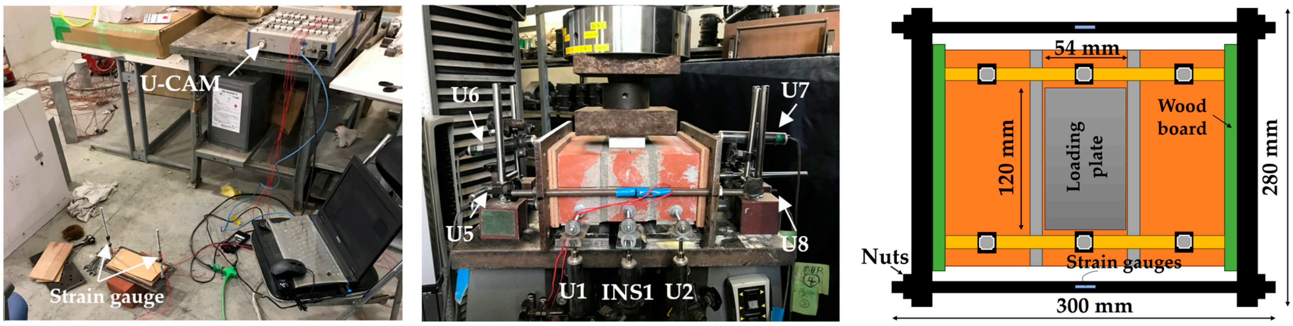

(**a**) Installation process (**b**) Laying specimens on the machine

Figure 11. Test set up for shear tests.

The interface is governed by cohesive frictional behavior, which was modeled using the Mohr–Coulomb failure criterion, illustrated in Equation (4) as

$$\tau = c + \sigma tan\varphi \tag{4}$$

where c is the cohesion coefficient in N/mm^2, σ is the pre-compression in N/mm^2, and φ is the friction angle in degrees.

4.3. Torsion Tests

Ten specimens were used for the torsional behavior tests. Two layers of brick in each specimen were staggered (half and half) and there was one layer of mortar, as listed in Table 5. The PP bands were used to strengthen five specimens, and the other five were not strengthened (Figure 12). Strengthening for the specimen with PP bands was performed similarly to that in the flexural test. The ultimate torsional strength was calculated using Equation (5) [30,31], as

$$\tau = \frac{P \times L}{b^2 \times \left(a - \frac{b}{3}\right)} \tag{5}$$

where τ is the ultimate torsional strength (N/mm^2), P is the ultimate load (N), a is the length of the mortar joint (mm), and b is the width of the brick (mm).

To measure the displacement of the specimen, two LVDTs (INS1 and INS2) were placed at the mid-span of the specimen at two lateral faces, as shown in Figure 13. They were connected to the INSTRON machine. The load rate was kept at 0.005 mm/s.

Table 5. Specimen dimensions in the torsion tests.

Numbers		Span L, mm	Length a, mm	Width b, mm
TN-1	Non PP band	262	105.0	100.0
TN-2		263	106.4	100.5
TN-3		260	105.3	100.0
TN-4		262	105.5	99.80
TN-5		266	105.2	100.0
TP-1	PP band	264	104.8	100.0
TP-2		263	105.0	101.2
TP-3		265	106.5	101.6
TP-4		266	106.0	100.0
TP-5		267	104.5	100.0

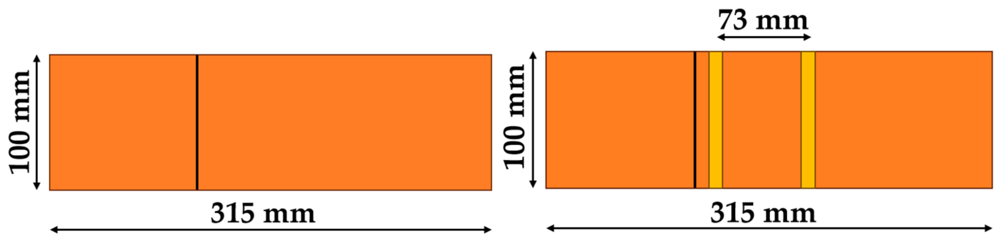

Figure 12. Non-PP band specimen and PP band specimen.

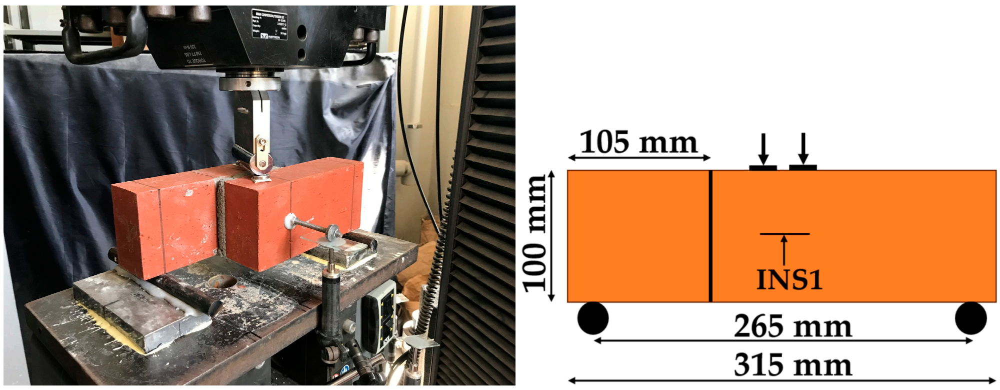

Figure 13. Test set up for torsion tests.

5. Results and Discussion

5.1. Flexural Tests

Load–deflection relationships of unreinforced specimens at the center are displayed in Figure 14a. The failures of the unreinforced prism specimens were sudden and brittle. Most prism specimens were split into two pieces (Figure 15a). The failure of the specimen was caused by a crack that appeared near either side of the loading steel rod. The average peak flexural strength, average deflection, and average load-carrying capacity of the specimens at the center were 0.343 N/mm^2, 0.026 mm, and 0.163 kNm, respectively (Table 6).

The experiment on the PP band-strengthened specimens showed that the PP bands effectively increased the collapse time of the specimens after the initial drop (Figure 14b). Residual loading was observed in all specimens and improvements in the load-carrying capacity and deflection ability were observed for the reinforced specimens. The average load-carrying capacity at ultimate failure and deflection at first crack of the PP band specimens were 1.70 times and 1.62 times (Table 6) higher than those of non-PP band specimens. Similarly, the deflection ductility clearly increased when compared to the non-PP band specimens, as listed in Table 6. The initial stiffnesses of the strengthened specimens were similar to those of unreinforced specimens. The secant stiffnesses showed marked decreases. The first cracks of the FP-1, FP-3, and FP-4 specimens were initiated between the steel rod loading lines, while those of the FP-2 and FP-5 specimens were outside of the steel rod loading lines (Figure 15c). The PP bands took the resistance due to a further increase in load only. The test was terminated when the link between the PP band and the washer was completely ruptured (Figure 15b). It was concluded that the proposed method produced the greatest improvements in the load-carrying capacity and deflection. This proves the effectiveness of the proposed method, although Ref [16] stated that the strength of the wall did not increase with the strengthening PP band.

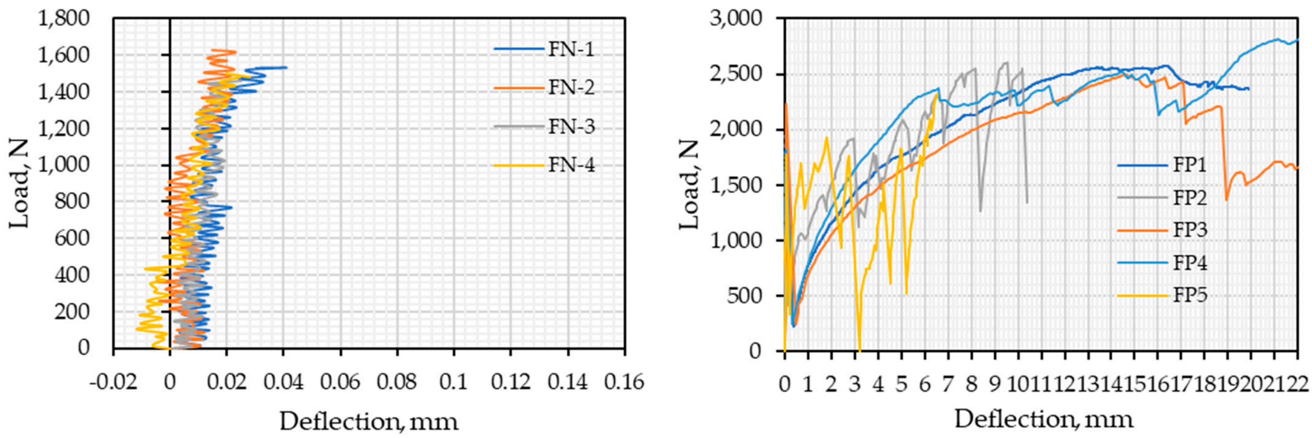

(**a**) Unreinforced prism specimens (**b**) Reinforced prism specimens

Figure 14. Load–deflection relationships of the unreinforced and reinforced specimens.

(**a**) Unreinforced prism specimen (**b**) Prism specimen FP1 (**c**) Prism specimen FP5

Figure 15. Failure patterns of the specimens with PP bands and non-PP band.

Table 6. Mechanical properties of the unreinforced and strengthened specimens in flexural tests.

Specimens	First Crack		Ultimate Failure		First Crack	Ultimate Failure	First Crack	Ultimate Failure	Deflection Ductility, Times	Average of Improvement, Times	
	Load, kN	Deflection, mm	Load, kN	Deflection, mm	Flexural Strength, N/mm^2		Flexural Moment, kNm			Deflection (First Crack)	Moment (First Crack and Ultimate Failure)
FN-1	1.53	0.041	-	-	0.34	-	0.163	-	1.0	-	-
FN-2	1.63	0.016	-	-	0.36	-	0.173	-	1.0		
FN-3	1.46	0.025	-	-	0.33	-	0.155	-	1.0		
FN-4	1.50	0.020	-	-	0.34	-	0.159	-	1.0		
Ave.	1.53	0.026	-	-	0.343	-	0.163	-			
FP-1	1.99	0.042	2.58	16.38	0.44	0.57	0.216	0.280	390	1.62	1.28 and 1.70
FP-2	1.85	0.040	2.61	9.53	0.39	0.55	0.198	0.279	238		
FP-3	2.23	0.035	2.49	14.65	0.46	0.51	0.234	0.262	419		
FP-4	1.82	0.039	2.83	22.09	0.40	0.61	0.196	0.304	566		
FP-5	1.77	0.054	2.32	6.55	0.40	0.52	0.194	0.254	121		
Ave.	1.93	0.042	2.57		0.418	0.552	0.208	0.276			

5.2. Shear Tests

Figure 16a illustrates the shear strength–slip curves for various values of pre-compression (σ) for the unreinforced specimens. As observed, the shapes of the curves depend on the level of pre-compression σ, with the shear strength τ increasing proportionally with σ. With each value of pre-compression (0, 0.2, 0.4, and 0.6 N/mm^2), the average ultimate shear strengths were obtained as 0.39 N/mm^2, 0.51 N/mm^2, 0.83 N/mm^2, and 1.22 N/mm^2, respectively, as shown in Table 7. Tests on the strengthened specimens (Figure 16b) showed increases in the shear strength for all pre-compression ranges of 0.2–0.6 N/mm^2, by 0.57 N/mm^2, 0.85 N/mm^2, and 1.29 N/mm^2, respectively (Table 8). However, they were not significant. The initial stiffnesses were not significantly affected by the pre-compression level in both the reinforced and unreinforced case.

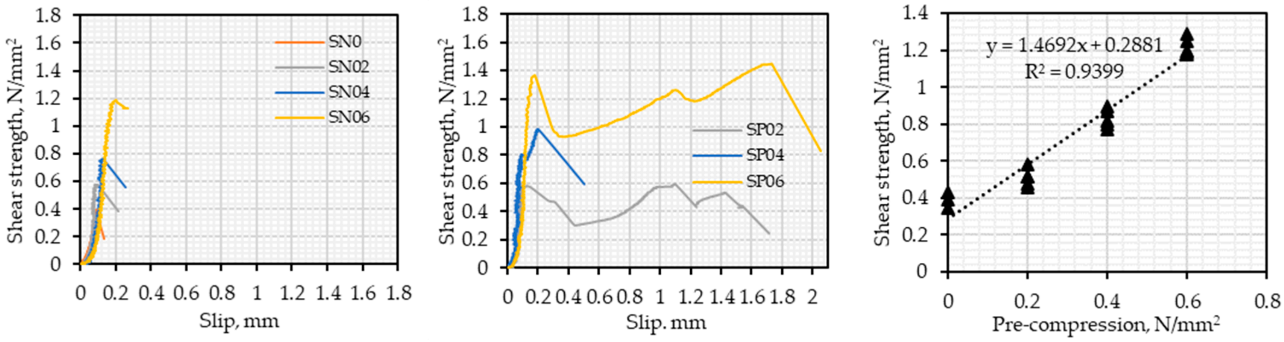

(**a**) Unreinforced specimens (**b**) Reinforced specimens (**c**) Shear stress vs. pre-compression

Figure 16. Shear stress–slip curves for the unreinforced and reinforced specimens and the relationship between shear stress and pre-compression stress.

Table 7. Mechanical properties of the unreinforced specimens in shear tests.

Specimens	Load, kN	Slip, mm	Pre-Compression σ, N/mm^2 or N	Shear Stress τ, N/mm^2	Stiffness, N/mm^3	Average of Shear Stress τ, N/mm^2	Average of Slip, mm
SN0-1	17.87	0.084	0	0.43	5.12	0.39	0.078
SN0-2	14.78	0.072		0.35	4.86		
SN0-3	16.33	0.077		0.39	5.06		
SN02-1	19.98	0.094	0.2 (4200 N)	0.48	5.11	0.51	0.102
SN02-2	24.47	0.101		0.58	5.74		
SN02-3	19.38	0.102		0.46	4.51		
SN02-4	22.01	0.116		0.52	4.48		
SN02-5	21.78	0.095		0.52	5.47		
SN04-1	34.29	0.128	0.4 (8400 N)	0.82	6.38	0.83	0.128
SN04-2	32.17	0.121		0.77	6.33		
SN04-3	38.00	0.129		0.90	7.01		
SN04-4	36.72	0.132		0.87	6.62		
SN04-5	33.49	0.130		0.80	6.13		
SN06-1	49.65	0.185	0.6 (12,600 N)	1.18	6.38	1.22	0.207
SN06-2	52.60	0.235		1.25	5.32		
SN06-3	54.47	0.208		1.29	6.20		
SN06-4	54.07	0.194		1.19	6.13		
SN06-5	50.43	0.211		1.20	5.69		

The failures of the unreinforced and reinforced specimens were shown in two stages. In the first stage, it was damaged at one of the four interfaces between the brick and mortar layer, where the bond between them was weaker. Afterwards, the load continued to increase until the second interface between the brick and mortar was destroyed. The increase was due to the pressure from the two sides maintained during the experiment. In reinforced specimens, the two lateral bricks tended to move inward, which meant that the two PP band-fixed points also moved, making the PP band slack. Consequently, we did not observe an increase in load and the load suddenly decreased. Hence, the role of the PP band in enhancing shear ability was not evident.

Table 8. Mechanical properties of the reinforced specimens in shear tests.

Specimens	Load, kN	Slip, mm	Pre-Compression σ, N/mm^2	Shear Stress τ, N/mm^2	Stiffness, N/mm^3	Average of Shear Stress τ, N/mm^2	Average of Slip, mm
SP02-1	26.94	0.126	0.2 (4200 N)	0.64	5.08	0.57	0.113
SP02-2	20.43	0.100		0.49	4.90		
SP02-3	24.57	0.108		0.59	5.46		
SP02-4	23.61	0.116		0.56	4.82		
SP04-1	37.24	0.133	0.4 (8400 N)	0.89	6.69	0.85	0.124
SP04-2	33.72	0.121		0.80	6.60		
SP04-3	36.54	0.128		0.87	6.80		
SP04-4	34.66	0.115		0.83	7.22		
SP06-1	55.62	0.223	0.6 (12,600 N)	1.32	5.92	1.29	0.235
SP06-2	51.54	0.203		1.23	6.06		
SP06-3	57.21	0.318		1.36	4.27		
SP06-4	53.34	0.196		1.27	6.48		

Moreover, failure patterns of the unreinforced specimens are displayed in Figure 17a–d. In cases of pre-compression (0, 0.2, 0.4 N/mm^2), cracks appeared at the mortar–brick interface, while with 0.6 N/mm^2, the observed failure mode was a combination of sliding along the mortar–brick interfaces and diagonal cracks appeared near the interface through the mortar layer. A minor crack was also observed propagating into the central brick at the peak load. The failure patterns of the reinforced specimens are also presented in Figure 17e–g. It was observed that the reinforced specimens with PP bands did not sustain failure mode changes, and cracks appeared at the mortar–brick interface in all cases of pre-compression. At 0.6 N/mm^2, cracks were also observed in the central brick.

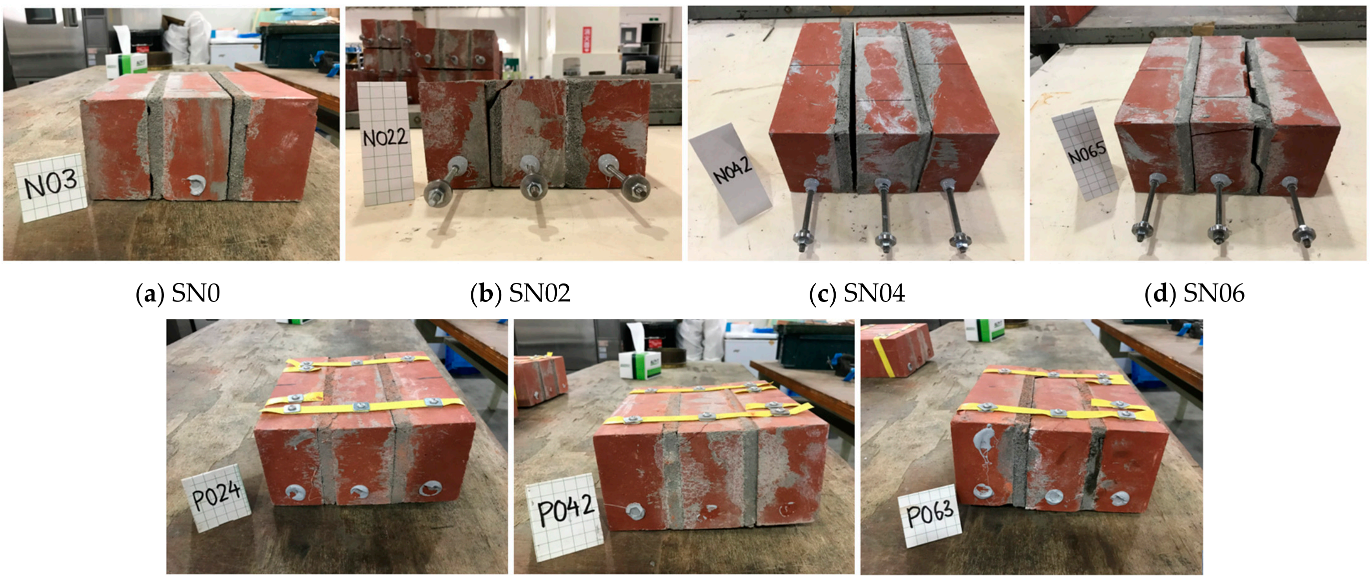

(**a**) SN0 (**b**) SN02 (**c**) SN04 (**d**) SN06

(**e**) SP02 (**f**) SP04 (**g**) SP06

Figure 17. Failure patterns of the shear specimens.

The results in terms of pre-compression and shear strength at failure, together with parameters such as the friction angle and cohesion of the mortar joint, were obtained from the linear interpolation in Figure 16c. The cohesion value (c) was equal to 0.288 and the slope of the linear interpolation (tan φ) indicated a friction coefficient of 1.469.

5.3. Torsion Tests

The load and deformation relationships of the unreinforced and reinforced specimens are presented in Figure 18, and the results are summarized in Table 9. The failures of the unreinforced specimens were sudden and brittle. The improvements in the average load-carrying capacity and deformation ability at first crack were 1.21 times and 1.47 times, respectively. The load suddenly dropped and no longer increased. The ductility evidently increased. Cracks occurred at the mortar–brick interface (Figure 19a,b). In the reinforced specimens, after failure, slight increases in load were observed in the TP-2, TP-3, and TP-5 specimens until the PP band's fixed positions were ruptured (Figure 19d). However, it did not exceed the peak load. This circumstance was not the same as that in the flexural test. However, the PP band effectively increased the collapse time of specimens. Unlike the cracks that appeared in the TP-2, TP-3, and TP-5 specimens, cracks in the TP-1 and TP-4 specimens appeared in both the brick and mortar layer and bricks (Figure 19c). This was because the strengthening method creating a pre-tensioning force appears in the PP band, helping to increase the load-carrying capacity of the reinforced specimen.

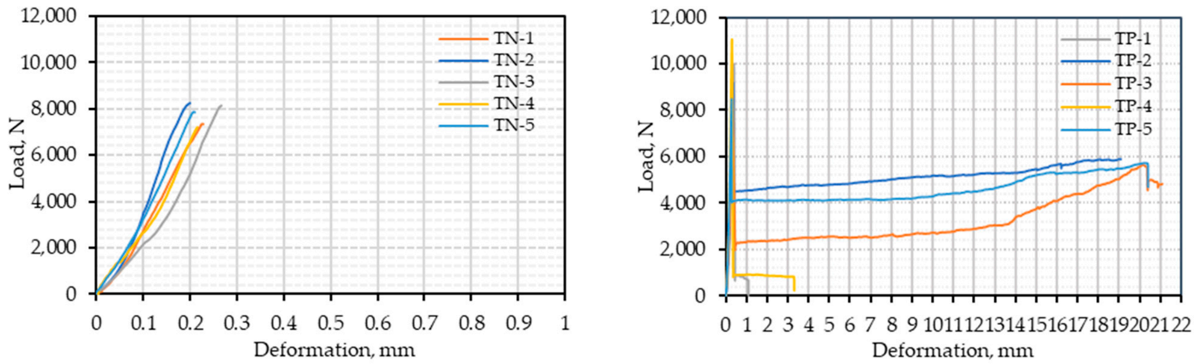

(**a**) Unreinforced specimens (**b**) Reinforced specimens

Figure 18. Load–deformation relationships of the unreinforced and reinforced specimens.

Table 9. Mechanical properties of the unreinforced and reinforced specimens in torsion tests.

Specimens	First Crack		Ultimate Failure		First Crack	Ultimate Failure	Deflection Ductility, Times	First Crack	Ultimate Failure	Average of Improvement, Times (First Crack)	
	Load, kN	Deformation, mm	Load, kN	Deformation, mm	Torsional Strength, N/mm²			Torsional Moment, kNm		Deformation	Moment
TN-1	7.37	0.225	-	-	1.17	-	1.0	0.98	-		
TN-2	8.24	0.200	-	-	1.31	-	1.0	1.09	-		
TN-3	8.13	0.267	-	-	1.29	-	1.0	1.08	-	-	-
TN-4	7.14	0.214	-	-	1.14	-	1.0	0.95	-		
TN-5	7.89	0.207	-	-	1.25	-	1.0	1.05	-		
Ave.	-	0.223	-	-	1.23	-	-	1.03	-		
TP-1	9.98	0.393	-	-	1.59	-	-	1.32	-		
TP-2	9.18	0.346	5.89	19.09	1.46	0.94	55	1.22	0.78		
TP-3	8.07	0.319	4.82	21.09	1.28	0.77	66	1.07	0.75	1.47	1.21
TP-4	11.06	0.297	-	-	1.76	-	-	1.46	-		
TP-5	8.49	0.282	5.71	20.38	1.35	0.91	72	1.11	0.75		
Ave.	-	0.327	-	-	1.49	0.87	-	1.24	0.76		

(**a**) Unreinforced specimen TN1 (**b**) (**c**) Reinforced specimen TP1 (**d**) Reinforced specimen TP5

Figure 19. Failure patterns of the torsion specimens.

6. Conclusions

A total of 49 specimens were tested to investigate the effectiveness of the PP band-fixing method on the flexural, shear, and torsion behaviors. Based on the observations of the experimental investigations, the following conclusions were drawn.

1. Strengthening the prism specimens with PP bands in the flexural tests significantly improved their performances in terms of load-carrying capacities and deflections at the first crack and ultimate failure that were the findings in this study. The PP band specimens showed 1.70 times and 1.62 times higher capacities than those of the non-PP band specimens. Improvements in the load-carrying capacity and deflection capacity were observed.
2. In the shear tests, the strengthened specimens represented negligible increases in the shear strength at the peak load for all pre-compression ranges of 0–0.6 N/mm^2. After the specimens were damaged, the load did not increase and gradually decreased. Therefore, the use of the PP band is not yet effective for strengthening triplet specimens under pre-compression.
3. In the torsion tests, improvements of 1.21 times and 1.47 times in the load-carrying capacity and deformation capacity at the first crack were observed, respectively. Nevertheless, at ultimate failure, the load-carrying capacity was lower than that at the first crack, even though PP bands were also effective in increasing the load. Thanks to PP band strengthening, the collapse times of the specimens were extended.
4. The proposed fixing method was effective in improving performances, restricting separation at the brick–mortar interface, and maintaining the specimens' integrity, particularly in the flexural tests.

Author Contributions: Conceptualization, Methodology, Data curation, Formal analysis, Investigation, Writing—Original draft preparation, T.Q.H.; Review, Funding acquisition and Editing, M.M.; Review, Editing, Y.T. All authors have read and agreed to the published version of the manuscript.

Funding: This research received no external funding.

Data Availability Statement: Data is contained within the article.

Acknowledgments: The authors wish to express their sincere gratitude to Yano (Muroran Institute of Technology, Japan).

Conflicts of Interest: The authors declare no conflict of interest.

References

1. The World Bank. *Vietnam Post-Typhoon Damrey Rapid Damage and Needs Assessment*; Khanh Hoa Provincial People's Committee: Hanoi, Vietnam, 2017.
2. News.abs-cbn.com. Over 60 Feared Dead after Typhoon Molave Slams into Vietnam. Available online: https://news.abs-cbn.com/overseas/10/30/20/over-60-feared-dead-after-typhoon-molave-slams-into-vietnam (accessed on 30 October 2020).
3. Takagi, H.; Thao, D.N.; Esteban, M. Tropical cyclones and storm surges in southern Vietnam. *Eng. Plan. Perspect.* **2014**, *2014*, 3–16.
4. Trinh, T.T.; Charitha, P.; Toan, B. The contribution of forerunner to storm surges along the Vietnam coast. *J. Mar. Sci. Eng.* **2020**, *8*, 508. [CrossRef]
5. Pandey, R.S.; Liou, Y.A. Decadal behaviors of tropical storm stacks in the North West Pacific Ocean. *J. Atmos. Res.* **2020**, *246*, 105143. [CrossRef]
6. World-habitat.org. Preventing Typhoon Damage to Housing, Central Vietnam. Available online: https://world-habitat.org/world-habitat-awards/winners-and-finalists/preventing-typhoon-damage-to-housing-central-viet-nam/#peer-exchange (accessed on 28 September 2008).
7. Lee, S. Disaster resilience of low-cost houses: Case study of Thua Thien Hue province. *J. Civ. Eng. Archit.* **2017**, *5*, 141–151. [CrossRef]
8. Babaeidarabad, S.; Arboleda, D.; Loreto, G.; Manni, A. Shearing strengthening of un-reinforced concrete masonry walls with fabric-reinforced-cementitious-matrix. *J. Constr. Build. Mater.* **2014**, *65*, 243–253. [CrossRef]
9. Bhattacharya, S.; Nayak, S.; Dutta, S.C. A critical review of retrofitting methods for unreinforced masonry structure. *Int. J. Disaster Risk Reduct.* **2014**, *7*, 51–67. [CrossRef]

10. Architectural Institute of Japan (AIJ). Technical Information for Disaster Mitigation of Masonry Structure. Available online: http://news-sv.aij.or.jp/kouzou/s5/fruit/Technical%20Information%20for%20Disaster%20Mitigation%20of%20Masonry%20Structures_20170309.pdf (accessed on 9 March 2017).
11. Al-Jaberi, Z.; Myers, J.J.; Elgawady, M.A. Out-of-plane flexural behavior of reinforced masonry walls strengthened with near-surface-mounted fiber-reinforced polymer. *ACI Struct. J.* **2018**, *115*, 997–1010. [CrossRef]
12. Al-Jaberi, Z.; Myers, J.J.; Elgawady, M.A. Experimental and analytical approach for prediction of out-of-plane capacity of reinforced masonry walls strengthened with externally bonded FRP laminate. *J. Compos. Constr.* **2019**, *23*, 04019026. [CrossRef]
13. Mayorca, P.; Meguro, K. Efficiency of polypropylene bands for the strengthening of masonry structures in developing countries. In Proceedings of the 5th International Summer Symposium, Japan Society of Civil Engineers (JSCE), Tokyo, Japan, 8 June 2003.
14. Mayorca, P.; Meguro, K. Proposal of an efficient technique for retrofitting unreinforced masonry dwellings. In Proceedings of the 13th World Conference on Earthquake Engineering, Vancouver, BC, Canada, 1–6 August 2004.
15. Bhattacharya, S.; Macabuag, J.; Gurgain, R. Seismic retrofitting of non-engineering masonry in rural Nepal. *Proc. Inst. Civ. Eng. Struct. Build.* **2012**, *165*, 273–286.
16. Umair, S.U.; Numada, M.; Amin, M.N.; Meguro, K. Fiber reinforced polymer and polypropylene composite retrofitting technique for masonry structure. *J. Polym.* **2015**, *7*, 963–984. [CrossRef]
17. Macabuag, J.; Bhattacharya, S.; Blakeborough, T. Extending the collapse time of non-engineered masonry buildings under seismic loading. In Proceedings of the 14th World Conference on Earthquake Engineering, Beijing, China, 20 February 2008.
18. Banerjee, S.; Nayak, S.; Das, S. Enhancing the flexural behavior of masonry wallet using PP band and steel wire mesh. *J. Constr. Build. Mater.* **2019**, *194*, 179–191. [CrossRef]
19. Velazquez-Dimas, J.I.; Ehsani, M.R. Modelling out-of-plane behavior of URM walls retrofitted with fiber composites. *J. Compos. Constr.* **2000**, *4*, 172–181. [CrossRef]
20. Richard, D.J.; Jenes, B. Assessment of out-of-plane failure of non-engineering masonry wall due to storm surges. *Int. J. Geomate* **2019**, *17*, 1–7.
21. Willis, C.R. Design of Unreinforced Masonry Walls for Out-of-Plane Loading. Ph.D. Thesis, University of Adelaide, Adelaide, Australia, 2004.
22. Chang, L.-Z.; Rots, G.R.; Esposito, R. Influence of aspect ratio and pre-compression on force capacity of unreinforced masonry wall in out-of-plane two-way bending. *J. Eng. Struct.* **2021**, *249*, 113350. [CrossRef]
23. Vasconcelos, G.; Lourenco, P. Experimental characterization of stone masonry in shear and compression. *J. Constr. Build. Mater.* **2009**, *23*, 3337–3345. [CrossRef]
24. *JIS R 1250*; Common Bricks and Facing Bricks. Japanese Industrial Standards Committee: Tokyo, Japan, 2011.
25. *JIS R 2213*; Test Method for Modulus of Rupture of Refractory Bricks. Japanese Industrial Standards Committee: Tokyo, Japan, 1995.
26. *JIS R 5201*; Physical Testing Methods for Cement. Japanese Industrial Standards Committee: Tokyo, Japan, 2015.
27. *JIS Z 1527*; Polypropylene Band. Japanese Industrial Standards Committee: Tokyo, Japan, 2002.
28. *ASTM E518-03*; Standard Test Methods for Flexural Bond Strength of Masonry. American Society for Testing and Materials: West Conshohocken, PA, USA, 2010.
29. Binda, L.; de Vekey, B.; Acharhabi, A.; Baronio, G.; Bekker, P.; Borchelt, G.; Bright, N.; Emrich, F.; Forde, M.; Gallegos, H.; et al. RILEM TC 127-MS. Tests for masonry materials and structures. *Mater. Struct.* **1996**, *29*, 459–475.
30. Hansen, K.F.; Pedersen, C.M. Torsion testing of bed joints. *Int. Mason. Soc.* **2008**, *21*, 10.
31. Hansen, K.F.; Pedersen, C.M. Shear and torsion testing of brick-mortar joints. *Int. Mason. Soc.* **2009**, *22*, 31–38.